Theoretical investigation into the effects of polar anchoring in antiferroelectric liquid crystal cells

N. J. Mottram[1] and S. J. Elston[2]
[1]*Department of Mathematics, University of Strathclyde, 26 Richmond Street, Glasgow G1 1XH, United Kingdom*
[2]*Department of Engineering Science, University of Oxford, Parks Road, Oxford OX1 3PJ, United Kingdom*
(Received 11 August 1999; revised manuscript received 23 May 2000)

We present a theoretical investigation into the effects of polar anchoring, which induces ferroelectric ordering close to the cell surfaces, in a liquid crystal cell containing an antiferroelectric liquid crystalline material. Our model includes effects due to finite polar and nonpolar anchoring, quadrupolar ordering and polarization self interaction. By minimizing the free energy of the system, we find parameter domains in which multiple zero-voltage solutions are stable. We find that these solutions may undergo thresholdless or hysteretic switching depending on the parameter values. In two instances, the presence of quadrupolar ordering or weak anchoring means that the cell must first be *primed* into the thresholdless state through a discontinuous transition from an initial antiferroelectric state.

PACS number(s): 61.30.Cz, 61.30.Gd

I. INTRODUCTION

Since the discovery of ferroelectric liquid crystals (SmC* or FLC) [1] and, some 13 years later, antiferroelectric liquid crystals (SmC_A^* or AFLC) [2], there has been considerable interest in the possibilities of using such materials in display devices. While FLC devices exhibit fast, inplane, bistable switching between two ferroelectric (F) states, AFLC devices have an additional, antiferroelectric (AF) state leading to the advantageous possibility of addressing a display symmetrically.

Recently, there has been an increased interest in thresholdless modes of operation of AFLC cells [3–5]. In such cells the material continuously transforms from the AF state to either of the F states upon application of an electric field. In liquid crystal devices such thresholdless switching modes have been of significant scientific and technological interest for some time. In nematic devices the hybrid aligned nematic cell [6,7] and the π cell [8] are operated in a thresholdless mode while for smectic devices the ferroelectric liquid crystal (FLC) deformed helix [9] and twisted FLC devices [10,11] and antiferroelectric liquid crystal (AFLC) materials [12] all exhibit thresholdless switching.

Although this type of switching is unfavorable in a passively addressed display, with active matrix addressing, i.e., using thin film transistor (TFT) technology, this mode has many advantages over bistable (or tristable) switching. The main advantage is that an analog grayscale can be reproduced so that in a color display a large number (theoretically an infinite number) of colors are possible.

While active matrix addressing has previously been avoided in FLC type display technologies due to the difficulties in mass production and expense, both of these problems have largely been overcome and device manufacturers are now willing to use TFT technology since the advantages outweigh the disadvantages.

The advantages of using AFLC materials (fast, in-plane, symmetric driving schemes, and large contrast ratio) led researchers to investigate the possibility of obtaining a thresholdless AFLC mode. In an apparently antiferroelectric (AF) material Inui *et al.* [12] observed a thresholdless mode that they explained in terms of a *random smectic* model where the director correlation between adjacent layers was small. However, recent experimental observations [3,4] suggest that a more realistic model for this behavior is a twisted smectic structure in which the AF ordering of the material is suppressed and the liquid crystal is in fact in the ferroelectric phase.

In many situations the cell must first be *primed* into the thresholdless state [3,5] by applying an electric field. After the cell has been primed it switches thresholdlessly. However, when the field is removed and the cell remains in the zero-voltage state for some time (which can be between hours and days) the *unprimed* ground state is recovered and the cell must first be primed again before thresholdless switching occurs.

In this paper, we develop a theoretical model of an AFLC cell in order to investigate the possible director configurations and how they switch when an electric field is applied. Specifically, we will consider the effects of confining surfaces that induce polar anchoring such that the material prefers to be in the F state at the cell boundaries. We show that the competition between F ordering at the surfaces and AF ordering in the bulk of the cell induces a coexistence of zero-voltage ground states. The identification of such ground states is extremely important when considering the switching characteristics in such cells. We find that due to the presence of quadrupolar ordering or weak anchoring, two modes of switching exhibit priming. The first of these modes is essentially that described by Rudquvist *et al.* [3] in which the thresholdless mode is simply the twisted smectic state described some years ago by Clark and Lagerwall [10] and Patel [11]. In this paper, we demonstrate how this thresholdless mode is primed from an AF state and, for an AFLC material, how the twisted smectic state can be stabilized by a quadrupolar ordering energy. In the second mode the dynamic ground state is a vertical AF state. This thresholdless AF switching mode was first described in a patent by Lee [13] and theoretically modeled by the present authors [14] while the zero-voltage ground state was previously discussed by Fournier [15]. In this paper, we describe how, due to finite polar and nonpolar anchoring, this state may be achieved from a uniform surface stabilized AF ground state.

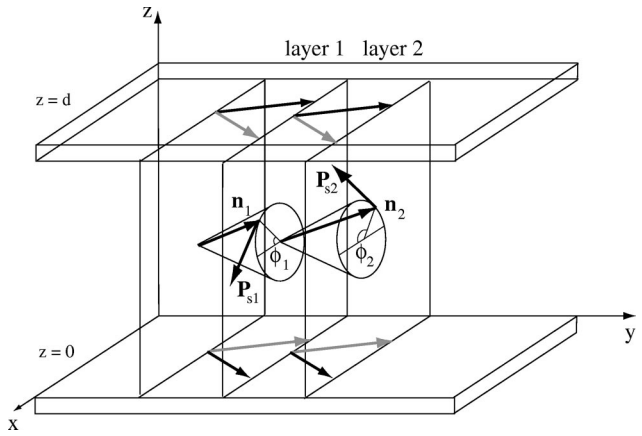

FIG. 1. Cell configuration: The directors, $\mathbf{n}_1$ and $\mathbf{n}_2$, in layers 1 and 2, respectively, lie on the smectic cone while the corresponding polarization vectors $\mathbf{P}_{s1}$ and $\mathbf{P}_{s2}$ lie in the xz plane perpendicular to the directors. The layers are in the bookshelf configuration between glass plates at $z=0$ and $z=d$. At the cell surfaces, the polar anchored director state (dark arrows) is the globally stable state while the antipolar anchored state (light arrows) is metastable.

In both of the above cases we are able to show how the thresholdless switching mode is primed from an initial AF state.

II. MODEL

The model used in this paper is an extension of our previous model [14] to include weak anchoring and quadrupolar ordering. We will assume that the smectic layers are in a bookshelf configuration and that the director within each layer lies on the smectic cone with a fixed cone angle (see Fig. 1). We also assume that the behavior may be modeled by only considering two adjacent smectic layers. This is equivalent to assuming that there is no helix present in the cell and thus the material is surface stabilized. The free energy of the smectic layers is then taken as the sum of energy contributions from electrostatic interactions, elastic deformation of the director, antiferroelectric and quadrupolar ordering within the liquid crystal, and both polar and nonpolar surface energies

At the cell boundary plates ($z=0,d$) the molecules prefer to lie on the cell surface rather than parallel to it. In other words, the director would like to lie on either side of the smectic cone ($\phi=0$ or π). However, since the materials that we are attempting to model have a high molecular spontaneous polarization ($|\mathbf{P_s}|\approx 5\times10^{-4}-1\times10^{-3}$ C/m^2), there will be a strong interaction between the surface alignment layer and the permanent molecular dipole. Thus the surfaces induce polar anchoring and the global surface energy minima is $\phi=0$ at $z=0$ and $\phi=\pi$ at $z=d$ while the other states are metastable minima. Such boundary conditions force the material to be in the ferroelectric phase at the surfaces.

If the director in each layer remains on a cone of angle θ and the layers are in the bookshelf configuration, then we can write $\mathbf{n}_i=(\sin\theta\cos\phi_i,\cos\theta,\sin\theta\sin\phi_i)$, where $i=1,2$ indicates the first or second layer and ϕ_i is the azimuthal director angle around the smectic cone. The corresponding spontaneous polarization vectors that lie perpendicular to $\mathbf{n}_i$ and the y axis are then $\mathbf{P}_{si}=P_s(\sin\phi_i,0,-\cos\phi_i)$. The free energy may be written as

$$\begin{aligned}\mathcal{F}=&\frac{\epsilon_0V^2}{2d\int_0^1\frac{1}{\epsilon_{zz}}dZ}-\frac{V\int_0^1\frac{P_z}{\epsilon_{zz}}dZ}{\int_0^1\frac{1}{\epsilon_{zz}}dZ}+\frac{d\left(\int_0^1\frac{P_z}{\epsilon_{zz}}dZ\right)^2}{2\epsilon_0\int_0^1\frac{1}{\epsilon_{zz}}dZ}\\&-\frac{d}{2\epsilon_0}\int_0^1\frac{P_z^2}{\epsilon_{zz}}dZ+\frac{K\sin^2\theta}{2d}\int_0^1\left[\left(\frac{d\phi_1}{dZ}\right)^2+\left(\frac{d\phi_2}{dZ}\right)^2\right]dZ\\&+\gamma d\int_0^1\cos(\phi_1-\phi_2)dZ-\gamma_q d\int_0^1\cos^2(\phi_1-\phi_2)dZ\\&+W_{np}[\sin^2(\phi_1(0))+\sin^2(\phi_2(0))+\sin^2(\phi_1(d))\\&+\sin^2(\phi_2(d))]+W_p[\sin^2(\phi_1(0)/2)+\sin^2(\phi_2(0)/2)]\\&+W_p[\cos^2(\phi_1(d)/2)+\cos^2(\phi_2(d)/2)],\end{aligned}\tag{1}$$

where $P_z=-P_s(\cos\phi_1+\cos\phi_2)/2$ and $\epsilon_{zz}=\epsilon_\perp+\Delta\epsilon\sin^2\theta(\sin^2\phi_1+\sin^2\phi_2)/2$ are the average spontaneous polarization in the z direction and the average zz component of the dielectric tensor. In Eq. (1), the z coordinate has been nondimensionalized with the cell gap width d so that $Z=z/d$, V is the voltage applied across the cell, $\epsilon_0=8.85\times10^{-12}$ F/m is the permittivity of free space, K is a Frank elastic constant, γ is the antiferroelectric ordering parameter, γ_q is the quadrupolar ordering parameter, W_{np} is the nonpolar anchoring strength, and W_p is the polar anchoring strength.

The first four terms in Eq. (1) describe the electrostatic energy contributions and are derived by solving Maxwell's equations [16] assuming that the electric properties may be averaged over the two layers. It has previously been shown that the presence of a spontaneous polarization in the layers causes a polarization self interaction that tends to minimize gradients in $\mathbf{P}_{si}$. Thus in a smectic-C twisted layer the bulk of the material will orient such that P_z is constant. However, since the electric properties have been averaged over two layers, the presence of AF ordering (i.e., $\phi_2=\pi+\phi_1$) leads to zero net polarization (i.e., $P_z=0$), and therefore it is possible to achieve a minimum in the electric energy with a nonuniform director profile as long as $\phi_2(z)=\pi+\phi_1(z)$.

The fifth term in Eq. (1) is the elastic distortion energy that may be thought of as the Frank elastic energy (under a one constant approximation) of the nematiclike directors within each layer. The sixth and seventh terms in Eq. (1) describe the liquid crystal material's tendency to form ferroelectric (F) or antiferroelectric (AF) states. When $\gamma>-2\gamma_q$, the AF state ($\phi_2=\pi+\phi_1$) is stable in the bulk material and when $\gamma<2\gamma_q$ the F state ($\phi_1=\phi_2$) is stable. When both states are stable ($-2\gamma_q<\gamma<2\gamma_q$) the AF state is the global energy minimum when $\gamma>0$; and the F state, when $\gamma<0$. In this paper, we will assume that we are below the smectic-C–smectic-C_A phase transition such that the F state is never the globally stable state but may be a metastable state.

The last terms in Eq. (1) are surface energies and govern the behavior of the director close to the cell surfaces. The nonpolar, W_{np} term describes the director's tendency to lie

on the cell surfaces ($\phi_{1,2}=0$ or π at $z=0$ or d). The polar, W_p term describes the polar interaction between the surfaces and the director such that at $z=0$ the directors prefer the orientation $\phi_{1,2}=0$ and at $z=d$ the directors prefer $\phi_{1,2}=\pi$ as discussed in the previous section.

The minimum energy equilibrium configuration may be found by solving numerically the Euler-Lagrange equations associated with the free energy (1) together with associated boundary conditions. For this minimization problem we employ the numerical continuation package AUTO97 [17,18] that will not only calculate a solution to the Euler-Lagrange equations but also investigate the behavior of this solution and the system as certain parameters vary.

For the dynamics of switching we use a relaxation technique that effectively solves the Ginzburg-Landau equation associated with the bulk energy in Eq. (1),

$$\mu\frac{\partial\phi_1}{\partial t}=-\mathcal{L}_{\phi_1}(F_{bulk}), \tag{2a}$$

$$\mu\frac{\partial\phi_2}{\partial t}=-\mathcal{L}_{\phi_2}(F_{bulk}), \tag{2b}$$

where F_{bulk} is the bulk free energy density associated with the nonsurface energy terms in $\mathcal{F}$, $\mathcal{L}_u=\partial/\partial u-d(\partial/\partial u_Z)/dZ$ is the normal Lagrangian operator, and μ is the viscosity of director motion around the smectic cone.

Using these two numerical methods, we are able to find the quasistatic hysteresis loop (AUTO97) and switching behavior (relaxation technique). The numerical details of these methods will not be discussed further in this paper.

This theoretical model is clearly extremely complex. There are many independent parameters and although some may be fixed to values typical for AF materials (we set $\epsilon_\perp=5.0$, $\Delta\epsilon=-1.5$, $\theta=25^o$, $P_s=5\times10^{-4}$ C/m^2, $\mu=100$ N s/m, and $K=10^{-11}$ N), we will want to alter other parameters in order to investigate the properties of the ground states and switching mechanism (i.e., the cell thickness d, the ordering parameters γ and γ_q, which will be temperature dependent, the anchoring strengths W_{np} and W_p, and of course the applied voltage V).

In the next section we investigate the effects of altering the cell thickness and AF ordering (when quadrupolar ordering is neglected and the surfaces induce strong polar anchoring) to find the ground states and switching behavior. In Sec. IV, we will concentrate on two points in parameter space in order to investigate the switching behavior and priming effect of two thresholdless modes. These two sets of parameters typify the behavior of the system in large regions of parameter space and small changes in the parameters do not qualitatively change the switching behavior of the cell.

III. GROUND STATES

In investigating the zero-voltage ground states of an AFLC cell, we simplify the above model. We will neglect the quadrupolar ordering term by setting $\gamma_q=0$, although we will reintroduce this term in Sec. IV. We will also assume that the cell surfaces induce strong polar anchoring (equivalent to setting $W_{np}=0$ and $W_p\to\infty$). It should be noted at this point that the mathematical description of polar anchoring in terms of the azimuthal angles ϕ_i is in fact degenerate. If the director is forced to lie on one side of the cone at one surface and on the opposite side of the cone on the other surface, the boundary conditions for the azimuthal angles are $\phi_i=2n_i\pi$ on $Z=0$ and $\phi_i=(2m_i+1)\pi$ on $Z=1$, where n_i and m_i are two (positive or negative) integers that may be different for each layer. Clearly there are an infinite number of possibilities. However, most of the possible values of n_i and m_i lead to director configurations that involve multiple rotations of the director around the cone. These solutions will contain a large amount of elastic energy and may be disregarded when compared to the two low-energy possibilities $n_1=n_2=0$, $m_1=m_2=0$ and $n_1=n_2=0$, $m_1=0$, $m_2=-1$.

From the form of the resulting dimensionless free energy (1) we see that the system is governed by only *two* dimensionless parameters $a=\epsilon_0\gamma/P_s^2$ and $b=\epsilon_0K\sin^2\theta/d^2P_s^2$. Whatever the values of the dimensional parameters (K, P_s, d, etc.), if a and b remain constant the equilibrium solutions will not change. There may be a multiplicative change in the free energy but this will not affect the stability or relative energies of the equilibrium solutions. We may therefore plot a phase diagram in terms of the two parameters a and b, which completely describes the system. However, it may be more useful to plot a phase diagram in terms of more meaningful and experimentally controllable parameters such as the cell thickness d and the F/AF ordering parameter γ, which will be related to the temperature.

Therefore, we initially fix all other parameters at the values previously mentioned ($\epsilon_0=8.85\times10^{-12}$ F/m, $\epsilon_\perp=5.0$, $\Delta\epsilon=-1.5$, $\theta=25^o$, $P_s=5\times10^{-4}$ C/m^2, and $K=10^{-11}$ N) but note that any change to these values will not qualitatively affect the d, γ phase diagram but will simply result in a rescaling of the d and/or the γ axes. For example, we note that the parameter transformation $(d,\gamma,P_s)\to(d/\alpha,\alpha^2\gamma,\alpha P_s)$, for any constant α leaves the free energy unchanged. Thus, a change in the value of P_s (i.e., $P_s\to\alpha P_s$) will simply alter the scales of the d and γ axes ($d\to d/\alpha$ and $\gamma\to\alpha^2\gamma$).

Figure 2 shows examples of the five solutions we obtain from minimizing the free energy at different γ values. The first three result from the first set of boundary conditions described above [$\phi_1(0)=\phi_2(0)=0$, $\phi_1(d)=\phi_2(d)=\pi$], which we denote by F_1 [Fig. 2(a)], AF_1 [Fig. 2(b)], and AF_2 [Fig. 2(c)]. The last two solutions result from the second set of boundary conditions described above [$\phi_1(0)=\phi_2(0)=0$, $\phi_1(d)=\pi$, $\phi_2(d)=-\pi$], which we denote by F_2 [Fig. 2(d)] and AF_3 [Fig. 2(e)].

In the F_1 solution, the liquid crystal exhibits ferroelectric ordering, i.e., $\phi_1=\phi_2$. The director continuously twists around the smectic cone from one cell boundary to the other. There is a concentration of the director twist near to the boundaries since, in the bulk of the cell, the electrostatic energy term disfavors variations of P_z. For smaller values of d, the twisted boundary regions become more dominant and the director tends to be more uniformly twisted across the cell. This solution has been previously investigated in detail and has been shown to undergo thresholdless switching and therefore exhibit an analog grayscale [11,19].

The two solutions AF_1 and AF_2 both exhibit antiferro-

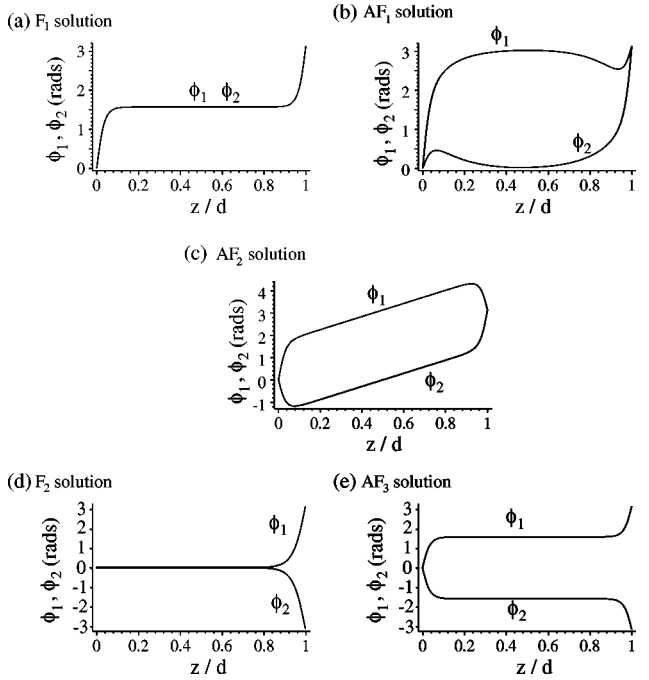

FIG. 2. Examples of the five zero-voltage, equilibrium solutions of the azimuthal angles ϕ_1 and ϕ_2 for parameter values $d=10^{-6}$ m, $P_s=5\times10^{-4}$ C/m^2, $K=10^{-11}$ N, $\theta=25^o$, $\epsilon_0=8.85\times10^{-12}$ F/m, $\Delta\epsilon=-1.5$, and $\epsilon_\perp=5.0$ and (a) $\gamma=0$, (b and c) $\gamma=30$, (d) $\gamma=-10$, (e) $\gamma=30$. (a) The F_1 solution for which $\phi_1=\phi_2$. (b) The AF_1 solution for which, in the bulk of the cell, $\phi_1\approx\pi$, $\phi_2\approx0$. (c) The AF_2 solution for which, in the bulk of the cell, $\phi_1=\phi_2+\pi$ but the directors in each layer uniformly rotate around the cone from one side of the cell to the other. (d) The F_2 solution for which $\phi_1=\phi_2$ in the bulk of the cell. (e) The AF_3 solution for which, in the bulk of the cell, a *vertical* AF state exists where $\phi_1=\pi/2$, $\phi_2=-\pi/2$.

electric ordering in the bulk of the cell (i.e., $\phi_1=\phi_2+\pi$) although the director configurations are somewhat different. In the AF_1 solution, the directors in the bulk of the cell are fixed approximately parallel to the cell surfaces ($\phi_1\approx\pi$, $\phi_2\approx0$), and near to the surfaces the directors reorient to satisfy the polar anchoring conditions. In the AF_2 solution the directors, while remaining in an AF state, continually twist around the cone from one surface to the other. An important feature of this solution is that there is no ''flattening'' of the azimuthal angle configuration, as in the F_1 solution, since in the AF state $P_z=0$ and thus the electrostatic free energy is automatically minimized.

In the last two solutions F_2 and AF_3, the bulk of the cell is in an F state ($\phi_1=\phi_2=0$) or an AF state ($\phi_1=\pi/2$, $\phi_2=-\pi/2$, i.e., the directors are in the vertical yz plane) while near to one or both cell surfaces the director reorients, in a narrow boundary region, to satisfy the boundary conditions. For $\gamma<0$, when the bulk of the cell prefers the F state, the F_2 solution is of lower energy than the AF_3 solution but of higher energy than the F_1 solution. For $\gamma>0$, when the bulk material prefers the AF state, the AF_3 solution is *always* the lowest energy configuration of all the solutions in Fig. 2. However, even though the AF_3 solution is the global energy minimizer in a large part of parameter space, at first sight it seems that this solution will be difficult to produce. In one layer the director rotates around the smectic cone in a clockwise direction while in the adjacent layer the director rotates in an anticlockwise direction. If the cell has been cooled down into the AF phase from the F phase, where the director configuration would prefer that of the F_1 solution [Fig. 2(a)] with the directors rotating around the cone in the *same* direction, the strong anchoring condition would prohibit the formation of the AF_3 state. However, we will show in Sec. IV that this low-energy state *is* accessible when the strong anchoring condition is relaxed and surface director switching can occur.

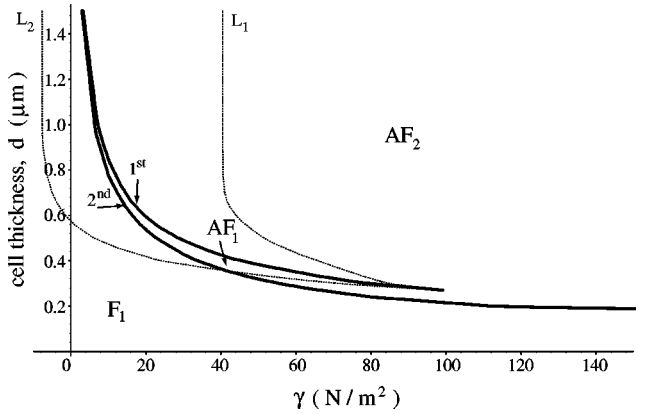

FIG. 3. The phase diagram for the existence and stability of the three solutions F_1, AF_1, and AF_2. The solid bold lines indicate the second-order transition between the F_1 state and an AF state and the first-order transition between the AF_1 and AF_2 states. The dotted lines L_1 and L_2 are the spinodal lines associated with the first-order transition that mark the absolute stability boundaries of the AF_1 and AF_2 states, respectively.

We now concentrate on the relative stabilities of the first three solutions F_1, AF_1, and AF_2. Figure 3 shows the phase diagram for these solutions. The solid bold lines denote a second-order transition between the F_1 state and an AF state and a first-order transition between the two AF states. The dotted lines denote the spinodal points associated with the first-order transition, i.e., the limits of metastability of the two AF phases. The labels F_1, AF_1, and AF_2 indicate the areas of the phase diagram in which each of the first three solutions in Fig. 2 are the lowest energy.

Below and to the left of the second-order transition line, the F_1 solution is the lowest-energy solution. This transition line asymptotes to $\gamma=0$ as $d\to\infty$ and to $d=0$ as $\gamma\to\infty$. This is to be expected when a is small compared to b and thus the AF ordering energy term is small compared to the electrostatic and/or the elastic energy terms. When the AF ordering term and the elastic term are comparable we have $a\sim b$ and thus $\gamma\sim K/d^2$ that agrees with the form of the second-order transition line.

As the second-order transition line is crossed, the F_1 state becomes unstable to a perturbation that destroys the F ordering in the bulk of the cell. The directors in adjacent layers (in the middle of the cell) move apart and thus one of the AF solutions is formed. For low values of d it is the AF_2 solution and for higher values of d it is the AF_1 solution. However, the AF_1 solution is only the lowest-energy configuration within a narrow region of the phase diagram. As d or γ increases, this solution becomes unstable to the AF_2 solution through a first-order transition (the solid bold line in Fig. 3

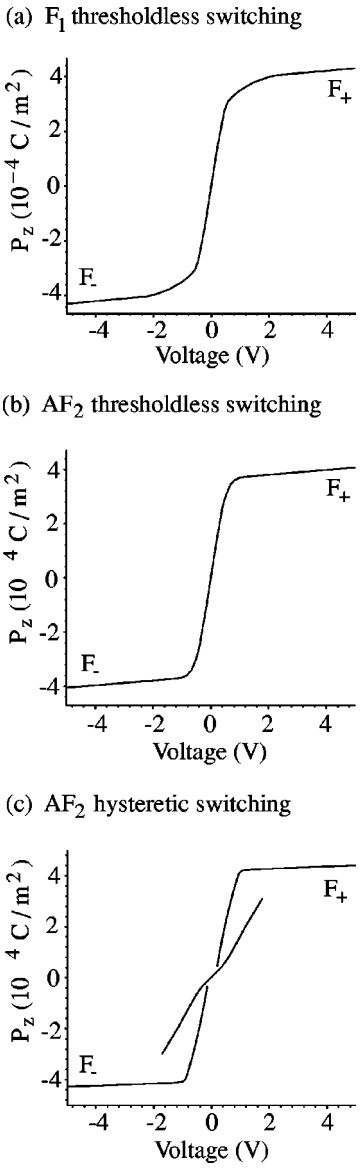

FIG. 4. Polarization P_z (averaged over the cell) versus voltage for (a) $d=0.2\times10^{-6}$ m, $\gamma=0$; (b) $d=0.2\times10^{-6}$ m, $\gamma=150$; (c) $d=0.5\times10^{-6}$m, $\gamma=150$.

indicated by the 1st label). The instability of the AF_1 solution is due to the high elastic energy regions close to the cell boundaries that, for large d and γ, are of higher energy than the continuous distortion present in the AF_2 solution.

The spinodal lines in the phase diagram denote the limits of *absolute* stability of the two AF states. Between the first-order transition line and L_1 in Fig. 3, the AF_1 solution is metastable, while between the first-order transition line and L_2, the AF_2 solution is metastable. The two spinodal lines meet as the first-order transition line terminates at a critical point. For large values of d the first-order transition line asymptotes to the second-order transition line, reducing the region in which the AF_1 solution is the globally stable state while the spinodal lines asymptote to fixed values of γ.

Having found the zero-voltage ground states, we now consider the switching behavior at three points in the phase diagram. Figure 4 shows P_z, the polarization in the z direction (averaged over the cell) as the voltage is varied for the points in the phase diagram, $d=0.2\times10^{-6}$ m, $\gamma=0$ [Fig. 4(a)], $d=0.2\times10^{-6}$ m, $\gamma=150$ [Fig. 4(b)], $d=0.5\times10^{-6}$ m, $\gamma=150$ [Fig. 4(c)]. For large positive voltages the electric field will cause the directors to lie on one side of the cone forming a ferroelectric state that we call F_+ (positive average P_z) while for large negative voltages the directors will lie on the other side of the cone in the F_- state (negative average P_z).

The F_1 solution has been previously investigated in detail and has been shown to undergo thresholdless switching, as in Fig. 4(a), and therefore exhibits an analog grayscale [11,19]. More interestingly, Figs. 4(b) and (c) show that the AF_2 state may switch thresholdlessly *or* hysteretically. At low values of d the AF state is not fully formed in the center of the cell and the cell switches continuously to the F_+ or F_- state. For d greater than about 0.3×10^{-6} m, the cell switches hysteretically between the fully formed AF state and the switched state. In a similar way the AF_1 switches hysteretically, away from the F_1-AF_1 transition line, and thresholdlessly, close from the F_1-AF_1 transition line.

We now return to the remaining solutions, the AF_3 and F_2 states. As shown previously in Ref. [14], the AF_3 solution switches thresholdlessly. In this case, in the bulk of the cell the material is in the vertical AF state with the polarization vectors parallel to the cell surfaces. When an electric field is applied and there is no quadrupolar energy term the polarization simply rotates to align with the field direction (this form of switching will be further investigated in the next section). Since the F_2 state is always of higher energy than the F_1-state we do not consider it further although it can be shown that this state may switch hysteretically or thresholdlessly.

We have therefore found only two ground states that will switch thresholdlessly over large regions of parameter space, the F_1 and AF_3 solutions. However, these solutions have certain problems when considering experimental details. Firstly the F_1 solution was assumed to be the explanation of the switching mechanism in a cell at a temperature below the bulk F-AF transition temperature [3] and unless the cell is extremely thin, the F_1 state will be unstable. Then show in the next section that a quadrupolar ordering term will stabilize the F state and may explain the experimental results. As previously mentioned, the AF_3 state may be difficult to achieve due to the counter-rotating director structures in adjacent layers. We again show in the next section how this thresholdless switching state may be achieved by breaking the anchoring constraints at the cell surfaces.

IV. PRIMING

In this section, we investigate how it is possible to produce thresholdless switching in a cell at a temperature in which the bulk material would be in the AF state. We consider the two solutions F_1 and AF_3 that have been shown to exhibit thresholdless switching in large areas of parameter space.

Firstly, we consider the F_1 solution. In order to at least locally stabilize the F state at a low temperature, a quadrupolar energy term must be introduced. We start in the lowest-energy state for the boundary conditions [AF_2, Fig. 2(c)] and, once switched, the system can remain in the F state and

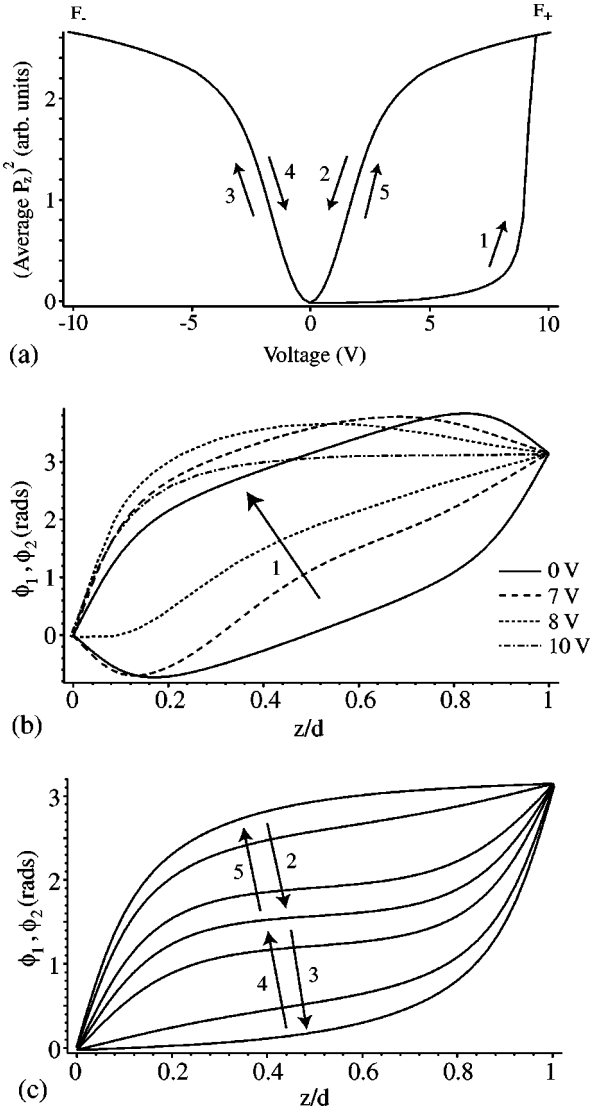

FIG. 5. Priming to, and thresholdless switching of, the twisted smectic state. (a) The polarization in the z direction, averaged over the cell thickness, squared, versus voltage. (b) Initial switching from the AF state to the F state. These ϕ_1 and ϕ_2 solutions correspond to states along the response branch numbered 1 in (a). (c) Thresholdless switching of the twisted smectic state where the solutions for ϕ_1 and ϕ_2 overlap since $\phi_1 = \phi_2$.

then switch thresholdlessly as long as the quadrupolar ordering is large enough. This is shown in Fig. 5. For this calculation we have used the parameter values $d = 10^{-6}$ m, $\gamma = 10^3$ N/m^2, and $\gamma_q = 10^3$ N/m^2 and assumed that there exists strong polar anchoring at the surfaces $W_{np} = 0$ and $W_p \to \infty$ [i.e., the directors at the surface are fixed to be $\phi_{1,2}(0) = 0$ and $\phi_{1,2}(d) = \pi$]. It should be noted that if the strong anchoring condition is relaxed such that W_p is finite but large, the switching behavior remains qualitatively the same.

In Fig. 5(a), we have plotted the average polarization in the z direction, squared, versus voltage to illustrate how the cell is first primed to the positive voltage F state (F_+) and then switches thresholdlessly between the F states (F_+ and F_-).

As the field is initially increased, the ground AF state switches hysteretically to the F_+ state [indicated by arrow 1 in Fig. 5(a)] with the director configuration switching from the ground state [solid lines in Fig. 5(b)] to the switched state [dashed-dotted lines in Fig. 5(b)]. From this point the F state is metastable, due to the presence of quadrupolar ordering, and will switch thresholdlessly in the same way as a twisted smectic device [10,11] [indicated by arrows 2–5 in Fig. 5(a)]. In the bulk of the cell the director azimuthal angle changes continuously from $\phi = \pi$ to $\phi = 0$ through the zero-voltage ground state $\phi = \pi/2$ [Fig. 5(c)].

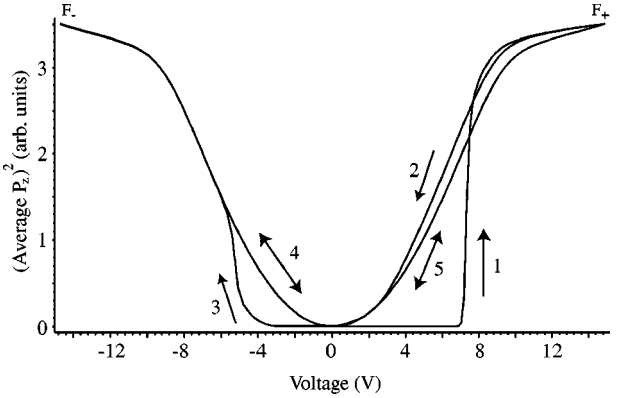

FIG. 6. Priming to, and thresholdless switching of, the vertical AF state. The polarization in the z direction, averaged over the cell thickness, squared, versus voltage. Solutions along these response branches are shown in Figs. 7–9.

If the voltage is removed, the F state remains but the system is in a high-energy metastable state. If the system is perturbed (by surface defects, regions of AF ordering etc.) The system reverts to the AF_2 ground state. We have confirmed this numerically by introducing a small numerical perturbation to allow the system to relax to the AF_2 state. Once the system has relaxed to the AF_2 ground state it will again prime into an F state upon application of a voltage and then switch thresholdlessly. Such an effect would agree with the experimentally observed behavior previously mentioned.

The second situation we consider is priming into the vertical AF thresholdless state, i.e., solution AF_3 [Fig. 2(e)]. We now demonstrate how this vertical AF state may be obtained

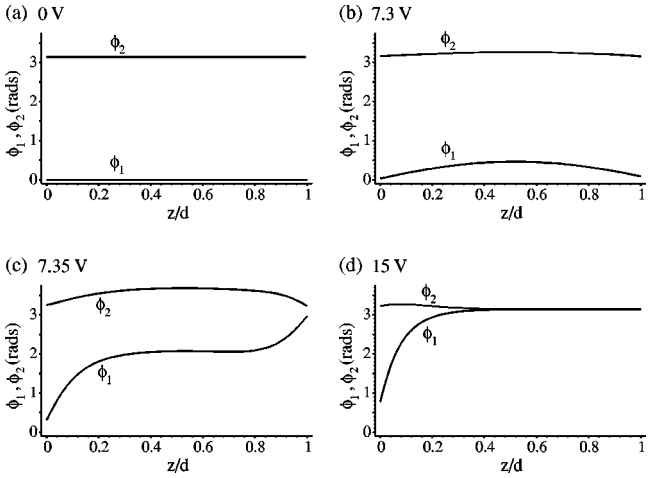

FIG. 7. Solutions along the first priming branch (labeled 1 in Fig. 6). Between $V = 7.3$ and $V = 7.35$, the anchoring breaks at one surface $z = d$.

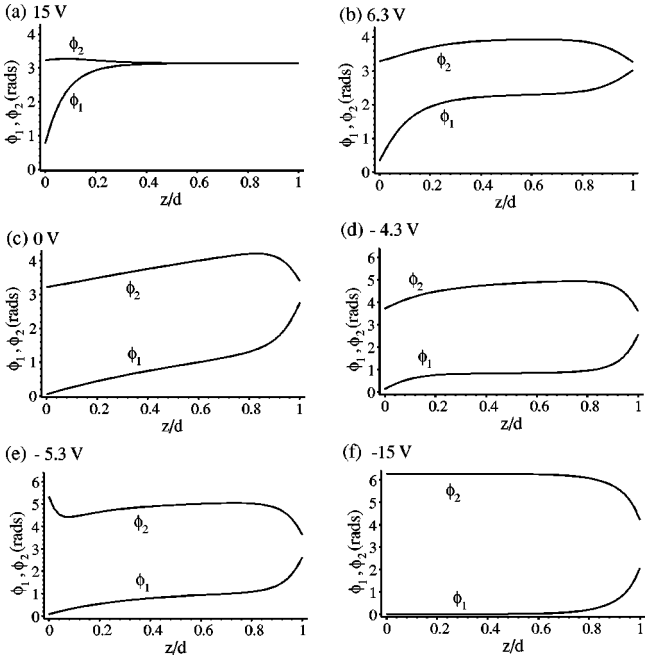

FIG. 8. Solutions along branches 2 and 3 (in Fig. 6). At $V=0$, an AF state exists where $\phi_2=\phi_1+\pi$ in almost all the cells. As the voltage becomes negative, the anchoring at the surface $z=0$ breaks (between $V=-4.3$ and $V=-5.3$) and the cell is almost completely in the F_- switched state.

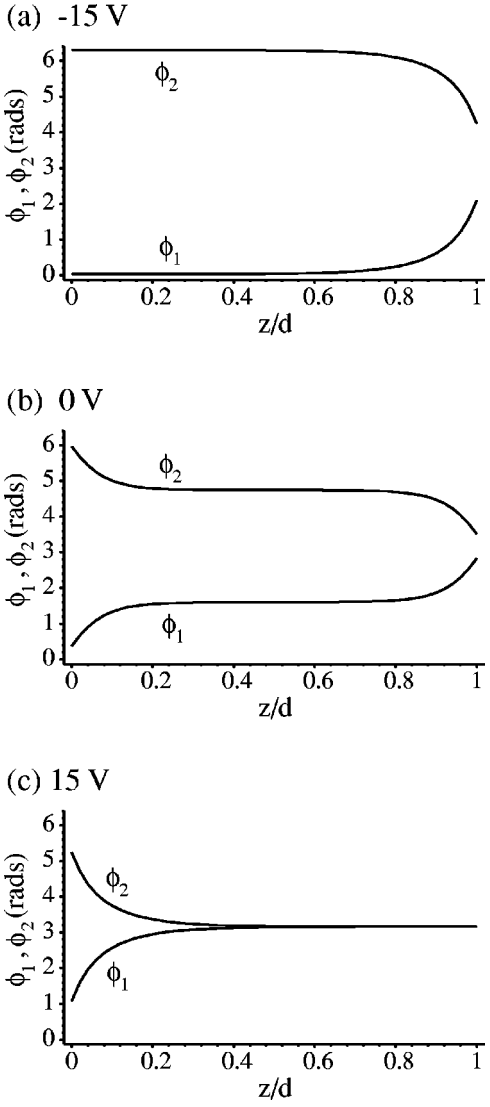

FIG. 9. Solutions along branches 4 and 5 (in Fig. 6). The cell has now primed into the vertical AF state for which switching is thresholdless. The cell cycles between the two F states (a) and (c) and the zero-voltage AF state (b).

from a uniform surface stabilized AF configuration. For this calculation we have used the parameter values $d=10^{-6}$ m, $\gamma=10^3$ N/m^2, and $\gamma_q=0$ so that there is no quadrupolar ordering and we assume that there is weak anchoring $W_{np}=1.5\times10^{-4}$ N/m, $W_p=1.5\times10^{-4}$ N/m, which means the polar anchored state is the global energy minimizer with a metastable antipolar state (see Fig. 1).

Figure 6 shows the response of the directors when, starting with a surface stabilized AF state ($\phi_1=0$, $\phi_2=\pi$), a triangular voltage waveform is applied. Figure 6 shows the average P_z response (squared) versus the applied voltage while Figs. 7–9 show the director angle response when switching from $0V$ to $15V$ (Fig. 7 and response branch 1 in Fig. 6), $15V$ to $0V$ [Figs. 8(a)–(c) and response branch 2 in Fig. 6], $0V$ — $15V$ [Figs. 8(c)–(f) and response branch 3 in Fig. 6(a)]. Figure 9 shows the thresholdless response once the cell has been primed (response branches 4 and 5 in Fig. 6).

Initially, when $V=0$, the directors are in the AF state $\phi_1=0$, $\phi_2=\pi$ [Fig. 7(a)]. At a critical voltage the bulk of the cell starts to switch to the F_+ state [Fig. 7(b)] and the surface anchoring at $z=d$ breaks [Fig. 7(c)] since the $\phi_1(d)=0$ state is only metastable while the $\phi_1(d)=\pi$ state is globally stable. At the maximum field value most of the cell is in the F_+ state ($\phi_{1,2}=\pi$) except for the anchored region where $\phi_1(0)$ is much smaller than π [Fig. 7(d)].

As the voltage is then reduced to zero, the directors relax to an AF state except near the anchored region at $z=d$ [Fig. 8(c)]. As the voltage further decreases to large negative values, the directors move toward the F_- state ($\phi_1=0$, $\phi_2=2\pi$) and the metastable anchoring $\phi_2(0)=\pi$ breaks [see Figs. 8(d) and (e)] and switches to the globally stable position $\phi_2(0)=2\pi$ [which is of course equivalent to $\phi_2(0)=0$].

From then on the cell switches thresholdlessly between the two F states (with surface reorientation regions induced by the anchoring conditions). In the zero-voltage ground state the bulk of the cell is in a vertical AF state, i.e. $\phi_1=\pi/2$, $\phi_2=3\pi/2$ (Fig. 9).

Thus there are two priming steps corresponding to the breaking of two surface anchoring conditions. It should be noted that for different parameter values, especially for smaller values of W_{np}, the second priming response may be very small.

As in the previous situation, the *primed* zero voltage state (the vertical AF state) may only be *metastable* for these parameter values. The original surface uniform AF state ($\phi_1=0$, $\phi_2=\pi$) may be the global energy minimizer and if the system was perturbed it would relax into the unprimed AF state. Priming would then be necessary to achieve thresholdless switching.

V. DISCUSSION

We have presented a theoretical model of switching in an AFLC material confined between surfaces that induce polar surface anchoring. Low-energy ground states have been found and their quasistatic switching investigated. For different parameters these configurations may exhibit thresholdless or hysteretic switching.

We have also demonstrated how two thresholdless switching modes may be primed from AF ground states. The first, a twisted smectic thresholdless mode, is stabilized below the smectic-C–smectic-C_A phase transition by the presence of a quadrupolar ordering term in the free energy. The second, a vertical AF thresholdless mode, is obtained from the uniform AF state by two priming steps that involve breaking of the anchoring constraints at each of the cell surfaces.

Although these two modes of switching are both thresholdless they will have different optical characteristics. In the first case the material is always ferroelectic and optically is a tilted uniaxial state whilst in the second case the material varies from an optically biaxial state at zero volts to a tilted uniaxial state for high voltages.

For this investigation of priming we looked at only two points in parameter space and although such modes exist for a relatively large range of parameters we have not explored the whole of the parameter space. Indeed the number of variable parameters makes it virtually impossible to fully investigate the system. However with the aid of detailed experimental results it will be possible to reduce the number and range of variable parameters. Specifically experimental techniques such as surface evanescent field [20] and guided mode [21] analyses will be extremely useful in determining the director behavior in the bulk and surface of the cell. The surface evanescent field technique will be particularly useful since it is able to probe the director structure near to the cell surface (between 100 Å and 1000 Å from the cell surface) and detect whether the surface switches between the AF and F states.

ACKNOWLEDGMENTS

The authors wish to thank Dr. M. J. Towler for useful discussions and the EPSRC and Sharp Laboratories of Europe Ltd., for financial support.

[1] R. B. Meyer *et al.*, J. Phys. (France) **36**, L69 (1975).
[2] A. D. L. Chandani *et al.*, Jpn. J. Appl. Phys., Part 2 **27**, L729 (1988).
[3] P. Rudquist, J. P. F. Lagerwall, M. Buivydas, F. Gouda, S. T. Lagerwall, N. A. Clark, J. E. Maclennan, R. Shao, D. A. Coleman, S. Bardon, T. Bellini, D. R. Link, G. Natale, M. A. Glaser, D. M. Walba, M. D. Wand, and X. H. Chen, J. Mater. Chem. **9**, 1257 (1999).
[4] B. Park, M. Nakata, S. Seomun, Y. Takanashi, K. Ishikawa, and H. Takezoe, Phys. Rev. E **59**, R3815 (1999).
[5] S. Seomun, Y. Takanishi, K. Ishikawa, H. Takezoe, and A. Fukuda, Jpn. J. Appl. Phys., Part 1 **36**, 3586 (1997).
[6] I. Dozov, P. Martinot-Lagarde, and G. Durand, J. Phys. (France) Lett. **43**, 365 (1982).
[7] G. Durand, F. Simoni, Appl. Phys. Lett. **44**, 504 (1982).
[8] G. D. Boyd, J. Cheng, and P. D. T. Ngo, Appl. Phys. Lett. **36**, 556 (1980).
[9] J. Fünfschilling and M. Schadt, J. Appl. Phys. **66**, 3877 (1989).
[10] N. A. Clark and S. T. Lagerwall, Ferroelectrics **59**, 25 (1984).
[11] J. S. Patel, Appl. Phys. Lett. **60**, 280 (1992).
[12] S. Inui, N. Iimura, T. Suzuki, H. Iwane, K. Miyachi, Y. Takanishi, and A. Fukuda, J. Mater. Chem. **6**, 671 (1996).
[13] S. D. Lee, U.S. Patent No. 5,784,140 (July 28th, 1998).
[14] N. J. Mottram and S. J. Elston, Liq. Cryst. **26**, 1853 (1999).
[15] J. Fournier, E. De Ley, B. Verweire and A. De Meyere, Mol. Cryst. Liq. Cryst. Sci. Technol., Sect. A **303**, 171 (1997).
[16] M. J. Towler, J. R. Hughes, and F. C. Saunders, Ferroelectrics **113**, 453 (1991).
[17] E. J. Doedel, Congressus Numeranti **30**, 265 (1981).
[18] E. J. Doedel and X. J. Wang, Center for Research on Parallel Computing, California Institute of Technology Report No. CRPC-95-2, 1995 (unpublished).
[19] Z. Zhuang, J. E. Maclennan, and N. A. Clark, Proc. SPIE **1080**, 110 (1989).
[20] J. Xue, N. A. Clark, and M. R. Meadows, Appl. Phys. Lett. **53**, 2397 (1988).
[21] F. Z. Yang, J. R. Sambles, and G. W. Bradbury, Liq. Cryst. **18**, 407 (1995).